CFD SIMULATION DESIGN AND UTILIZATION IN NATURAL GAS TREATING AND DISTRIBUTION

Engr. Nnadikwe Johnson[1], Engr. Ewelike Asterius Dozie[2], Ibe Raymond Obinna[3], Longinus mbakwem[4]

[1] *H.O.D in Department of Petroleum and Gas Engineering, Imo State University, Nigeria*

[2] *H.O.D in Agricultural Engineering, Imo State University, Nigeria*

[3] *Lecturer in department of Chemical Engineering, Imo State Polytechnic, Nigeria*

[4] *PhD. Research student , federal university of Port Harcourt. Rivers State, Nigeria*

ABSTRACT

Natural gas processing and transportation are two examples of CFD applications discussed in this chapter. For these experiments, researchers made use of the commercial program Fluent. Each study's goal, methodology, and boundary conditions and issue specifications are all briefly reviewed and quickly summarized. Research and comparisons using experimental testing and literature data are offered to illustrate how CFD may be used in real-world contexts.

Keywords: *CFD, Practical, Transportation, Processing*

1. INTRODUCTION

An increase in demand for natural gas has spurred exploration of distant offshore reserves by the energy sector. As a result, new methods for producing and transporting natural gas to points of consumption are required. The compactness and dependability of process equipment are common design issues in all gas processing technologies for offshore applications. Natural gas for offshore applications has been treated using supersonic nozzles to fulfill the needs of the industry (Hengwei et al. 2005, Alfyorov et al. 2005, Okimoto et al., 2002, Karimi & Abedinzadegan Abdi, 2006, Brouwer & Epsom, 2003). The gas temperature is decreased in a supersonic separator using the concept of gas expansion without the need of a refrigerant. In terms of natural gas treatment, the compact design of supersonic nozzles provides a significant benefit over previous methods. This device's gas speed is very high, thus particulates and ice can't foul or deposit on it. No heat is transported through the walls, and unlike external refrigeration systems, there is no need for an inhibitor injection and recovery mechanism for self-induced refrigeration. Cryogenic cooling or the use of solid adsorption methods are not necessary to obtain intense water dew points of -50 to -60 oC.

1.1 Definition of the issue

High-pressure natural gas flowing through supersonic nozzles may be predicted using CFD techniques. In the natural gas processing industry, it was found that supersonic nozzles may be used, although only a few modeling studies had been published in the open literature. We're looking at a de Laval nozzle here, which has two sections: a subsonic zone and a divergent zone (supersonic zone). The neck portion (critical zone) with an expanded constant area throat and the throat section with an extended U-shape throat are two further de Laval modified geometries of importance in solid/liquid particle separation.

The convergent section serves to maintain and accelerate the gas flow in a uniform and parallel manner. During the converging segment going to the throat, the gas is accelerated in order to attain the sonic velocity and maintain the gradient of flow uniform at the throat. Even if it may seem that the ratio of intake to throat diameters is less than 5 in certain circumstances, it is necessary to maintain the sonic speed to the throat under real settings (Man and colleagues, 1997). (Arina, 2004).

An outlet condition may affect how fast the gas travels through the diverging portion. Pressure and temperature fall as well as gas velocity rises due to this process. If the flow cannot expand isentropically to the exit pressure, then an irreversible discontinuity known as a shockwave may emerge as a result of the flow becoming isentropic.

Fluid parameters such as speed (from supersonic to subsonic), pressure, temperature, and density change abruptly and irreversibly as a result of a shockwave. Heat is transported and energy is disbursed throughout the gas as a consequence of the shock's temperature and velocity gradients, which are generated. There is no way to reverse these thermodynamic processes. To account for the insignificant loss of energy or heat, the cross sections at the upstream and downstream of the shock are assumed equal. There are several ways in which a shock might affect the boundary layer, and this can delay the transition even more. Increasing pressure over a shock indicates the shock strength that can produce a sound wave of minimal strength.

1.2 Basis of CFD simulation

Axisymmetric two-dimensional grids were used to represent the geometry. A complete pressure and temperature for fully developed turbulent flow were enforced at the nozzle input and no-slip conditions were implemented at the wall borders. The pressure and temperature of the surrounding air were measured at the departure point. Calculations were made using the SIMPLEC algorithm and the central differencing method.

The k- turbulent flow model was selected in this study because of its widespread usage in industrial applications, its correctness, and its inclusion in most commercial CFD software (Pope, 2000).

1.3 Results and discussions

1.3.1 de *Laval nozzles*

The Laval nozzle has dominated published research, therefore we used the numerical approach for this geometry and compared our results with the most current data (Arina, 2004; and Molleson & Stasenko, 2005) before moving on to the modified nozzle systems and putting our findings into action.

For their study, Molleson and Stasenko (2005a) used the nozzle geometry shown in Figure 1-a. Exit Mach number based on their supersonic exit radii (1.2) was determined to be 70 bar inlet stagnation pressure and 250 K inlet stagnation temperature for methane. The researchers in this study made use of the SRK EOS model. A thermodynamic model, such as MBWR, was employed in the comparison of sonic circumstances and in the investigation of how it affects the sonic position.

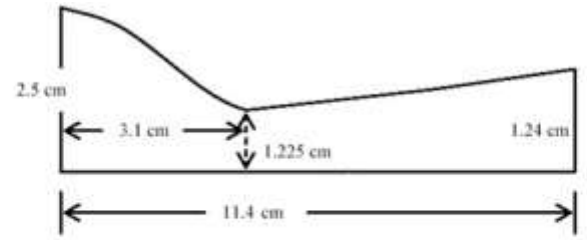

(a) (Molleson et al., 2005)

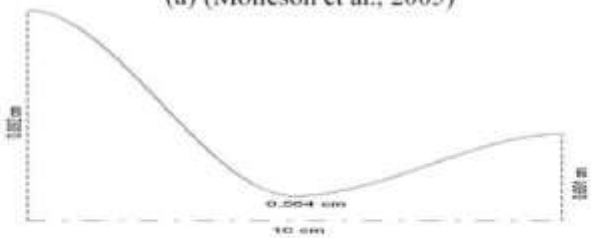

(b) (Arina, 2004)

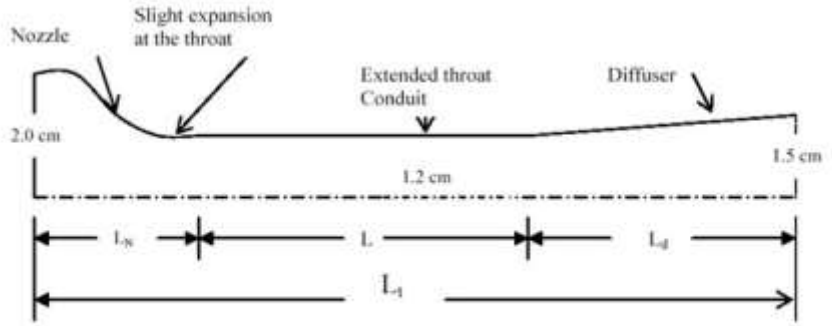

(c) System configuration for long-neck (long constant area/extended throat) Laval nozzle

Fig. 1. Nozzle geometries studied in the research

Figure 2 depicts the real-world variance in Mach number with respect to location, along with a comparison to the findings of Molleson and Stasenko's research (2005). Regardless of the EOS employed, the throat is where the choke (sonic velocity, M=1) occurs. In addition, our findings are pretty much in line with their findings. The second comparison was used to verify our simulation's ability to accurately capture the location of the shockwaves. With the most current data available, the comparison is made (Arina, 2004). As illustrated in Figure 1-b, Arina's geometry is employed in the comparison (2004). CO2 was used as the fluid in the machine. The Laval-dimensions nozzle's are as follows::

$$A(x) = 2.5 + 3\left(\frac{x}{x_{th}} - 1.5\right)\left(\frac{x}{x_{th}}\right)^2 \quad \text{for} \quad x \le x_{th}, \tag{1}$$

$$A(x) = 3.5 - \frac{x}{x_{th}}\left(6 - 4.5\frac{x}{x_{th}} + \left(\frac{x}{x_{th}}\right)^2\right) \quad \text{for} \quad x \ge x_{th}. \tag{2}$$

Where, A_{throat}= 1 cm^2, length= 10 *cm* and the throat placed at x_{th}= 5 *cm*.

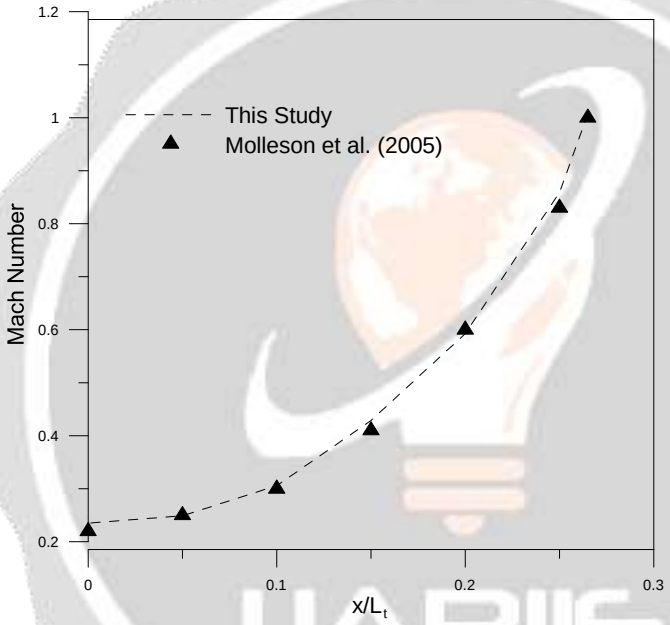

Fig. 2. Comparison of Mach numbers upstream of choke region in the Laval nozzle

The FLUENT real gas basis couldn't forecast multiphase conditions since Arina's simulation was run at T= 1.001Tc and = c, which are approaching CO2 condensation conditions. 83 percent of the inflow pressure was emitted. When the identical circumstances and working fluids were used as in Figure 3, our numerical findings showed the same behavior.

1.3.1.1 Real gas vs. Ideal gas assumption

Shockwave locations in the Laval nozzle may be more clearly shown by comparing methane and nitrogen gas models, as seen in the following figure. While the first compressibility factor drastically changes at high pressure, the second has practically the same compressibility as perfect gas at the same pressure.

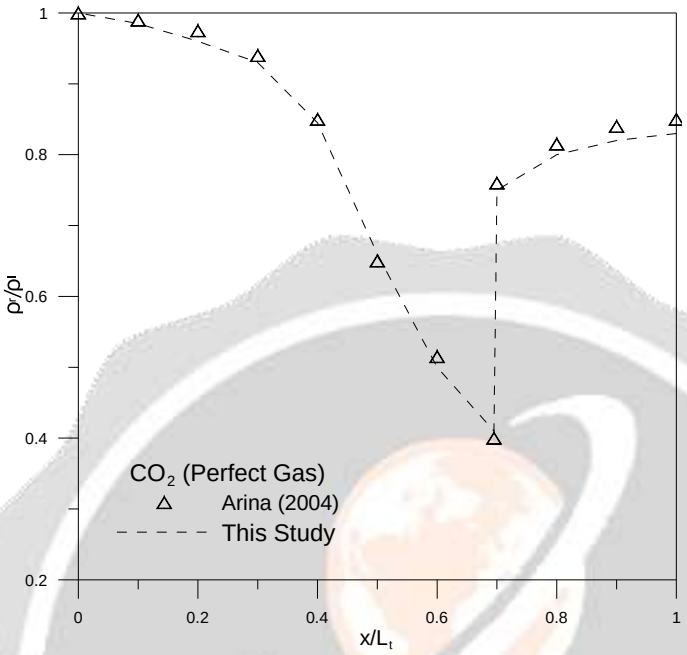

Fig. 3. Comparison of density ratios in the Laval nozzle under perfect gas conditions

1.3.1.2 Shockwave location

Shockwave location is better predicted by the actual gas model than by the ideal gas model for both gases. The ideal gas model. There is, however, a difference in the distance between the ideal and actual shock locations. Shock occurs early when the ideal gas model is applied (see Figure 4-a). Figure 4-b, on the other hand, shows that the actual gas model predicts an entirely different outcome. This is a good illustration of how neglecting the true impacts of gas may lead to inaccurate conclusions..

1.3.1.3 Real gas effects for a different configuration

An entrance nozzle (a converging portion that ends with a throat and expands somewhat), diffuser (a diverging portion that allows for the gas to expand fully and depart), and a conduit with a constant cross-section are the three components of the new nozzle system developed for natural gas applications. Then is no diffuser or diverging section after the throat in traditional Laval nozzles, which have a straight line from there to the exit point. Figure 1-c shows the new system's description.

The entrance pressure could be expected because of the way the boundary conditions were selected. For the inlet and outflow boundary conditions, we selected mass flow rate and temperature, whereas pressure and temperature were selected. Inlet and exit temperatures were 293 and 280 K, respectively, and outlet pressure was supposed to be 7 MPa. The mass flow rate was 430 kg/minute, and

the stagnation temperature and pressure were 293 and 280 K, respectively. We may have estimated the inlet's stagnation pressure. The following are some thoughts on the simulation's outcomes:

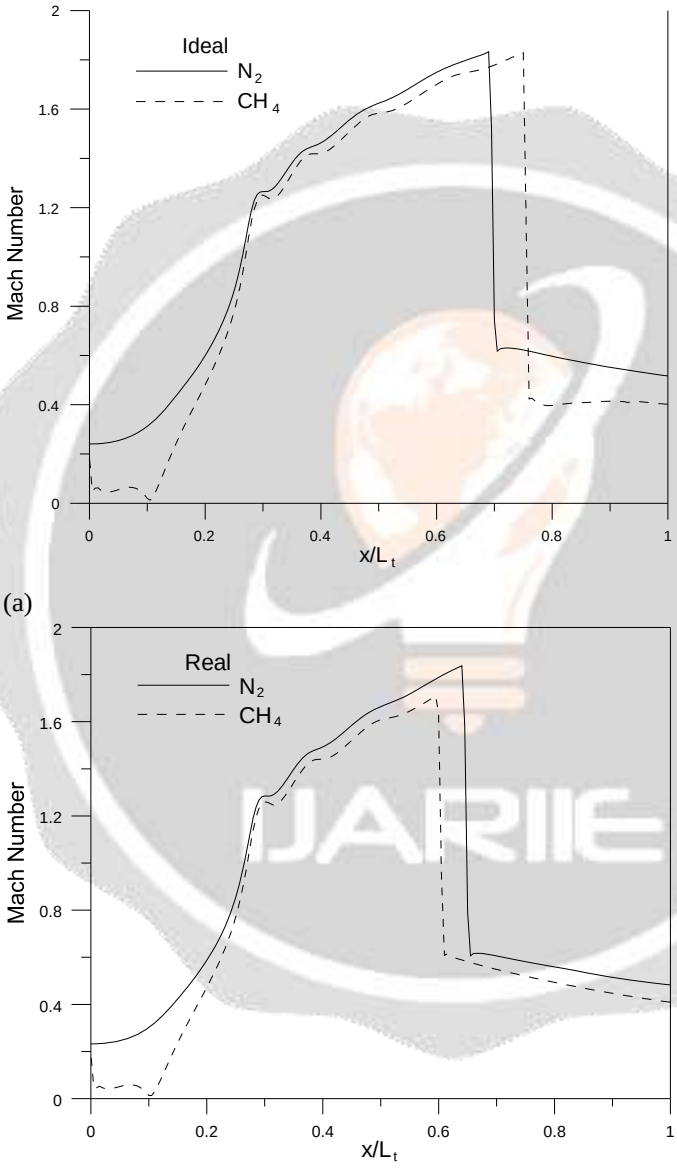

Fig. 4. Under ideal and actual gas circumstances, the shock location of nitrogen and methane are compared.

Density. The conservation of momentum equation has density terms in all of its components, as may be shown by consulting any fluid textbook. If the density calculation is incorrect, the flow structure will be adversely damaged. A graph of the density ratio (real/ideal) throughout the nozzle system is produced to show how this divergence affects the predictions in the nozzle (see Figure 5). When using a perfect gas model in the presence of a shockwave, it is clear how inaccurate the results might be. Near the shockwave, there is a noticeable increase in density fluctuations..

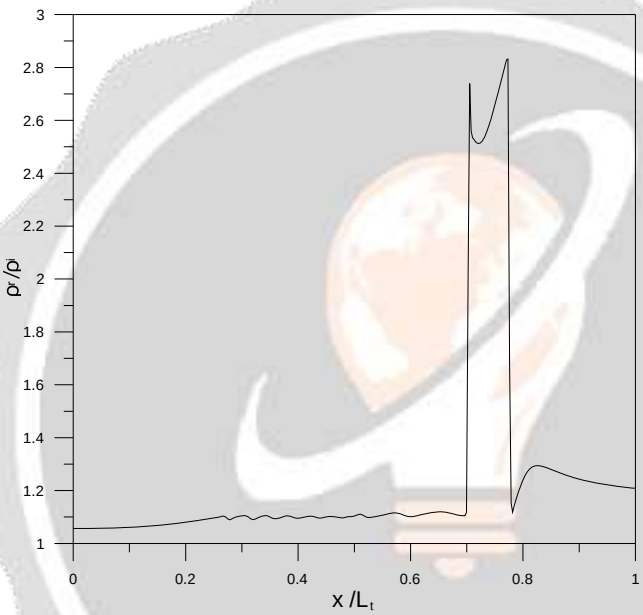

Fig. 5. In an expanded throat nozzle, the centerline density ratio is used to simulate actual gas (methane).

Inlet Pressure. For the mass flow rate, outlet pressure, and outlet temperature that we know, we can use our numerical solution to determine the input pressure. The distribution of static pressure along the axis is shown in Figure 6. At the intake pressure, one can clearly observe that the actual and ideal gas are quite different. For a given mass flow rate, the actual gas model forecasts a lower inlet pressure. A greater pressure recovery may be achieved as a result of this The ideal gas model forecasts pressure recoveries of 10% or more higher than what the actual gas simulation indicates. The estimate of total pressure diverges because of the discrepancy between actual and ideal static pressures. Incorrect estimations of friction loss, work, and heat transfer may result from inaccuracies in assessing the overall pressure and temperature. The total pressure and temperature predicted by ideal gas models and the actual ones are vastly different. Discrepancies in the data may lead to inaccurate estimates of friction losses and other variables.

Temperature. During the isentropic expansion process, the static temperature drops. The insulated wall's longitudinal static temperature change is seen in Figure 7. The actual gas example exhibits a greater drop in temperature than the ideal situation, as can be seen plainly here. Consequently, ideal gas simulation might provide incorrect findings when attempting to anticipate a possible phase transition in the material under consideration.

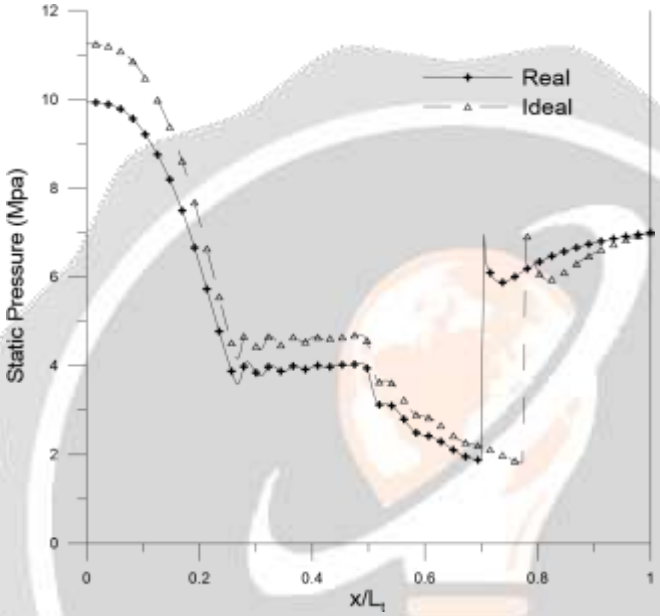

Fig. 6. An expanded throat nozzle with a centerline static pressure is used to simulate actual gas (methane).

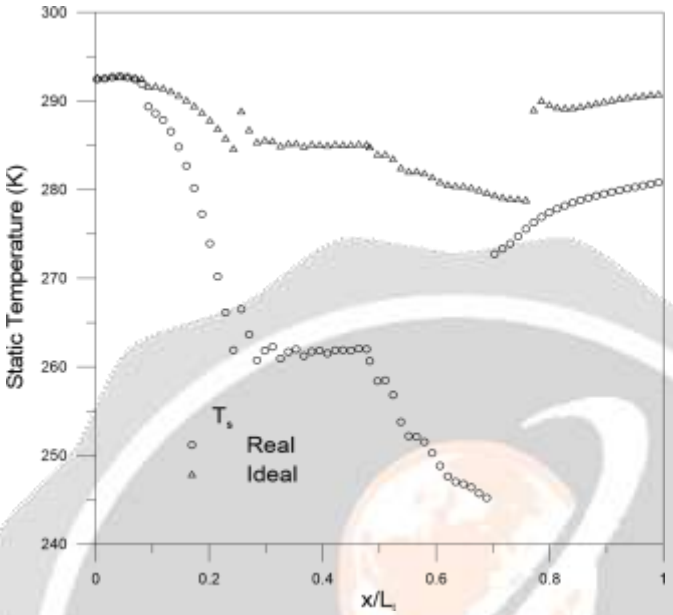

Fig. 7. For a genuine gas (methane) simulation in an expanded throat nozzle, wall static temperature distribution

When the nozzle is insulated, the stagnation temperature should remain constant. This is valid while using ideal gas law as thermodynamic model. However, the actual gas model predicts varying stagnation temperatures. In the actual gas scenario, the stagnation temperature fluctuates because the specific heat varies. Adiabatic Processes;

$$\int_{T_{01}}^{T_{02}} Cp(T_0).dT_0 = 0 \qquad (3)$$

This means that $T_{02} \neq T_{01}$ across the shockwave.

The choice of thermodynamic model may significantly alter the modelling results of supersonic nozzles utilizing actual gas models. This comprises shockwave position, fluid characteristics and circumstances, and work/heat transported throughout the system..

1.3.2 de *Laval nozzles* with extended straight throat

On the other hand, this section looks specifically at the effect of geometry on the gas flow through the supersonic nozzle. There are three parts to the nozzle (discussed in Segment 2.3.1): the convergent section, the expanded throat section, and the divergent section (supersonic zone).

Based on the conservation of mass, momentum, and the first and second principles of thermodynamics, the governing equations are obtained from the application of a very appropriate real gas Equation of State (EOS).

1.3.2.1 Geometry Influence

Choke location: It begins at the throat, expands somewhat in the slightly diverging/expansion part of the nozzle (about 0.04 meters), and then proceeds through the constant crosssection region, where shock occurs. After the shock, the flow becomes subsonic. As a result, pressure is restored. As a start It is believed that no condensation will occur when the gas travels through the nozzle due to the inability of Fluent simulation to forecast any phase shift. Real and ideal gas dynamics characteristics are shown in Figures 8. According to the illustration, there will be no noticeable changes in the longitudinal Mach number, notably in the inlet/converging region. The vertical line x=x* demonstrates that at the critical cross section of the nozzle, the Mach number is equal to one in both situations. This study's findings were in perfect agreement with what had been predicted (Arina, 2004, Molleson & Stasenko, 2005, and Drikakis & Tsangaris, 1993). So it may be deduced that sonic location is always near the throat, regardless of nozzle shape or gas thermodynamic model.

Shock position: A shock wave in the diffuser causes the flow to transition from supersonic to subsonic. Section 2.3.1 found that the actual gas model predicted the shock location sooner. Several actual gas EOS were compared to their ideal gas counterparts in Arina (2004). Convergent flow is predicted by all actual gas models, however shock location is somewhat different from one model to the next. Even at high pressures, inert gases (air) behave nearly perfectly thanks to a Laval nozzle and inert gases (such as nitrogen). Additionally, it's safe to say that.

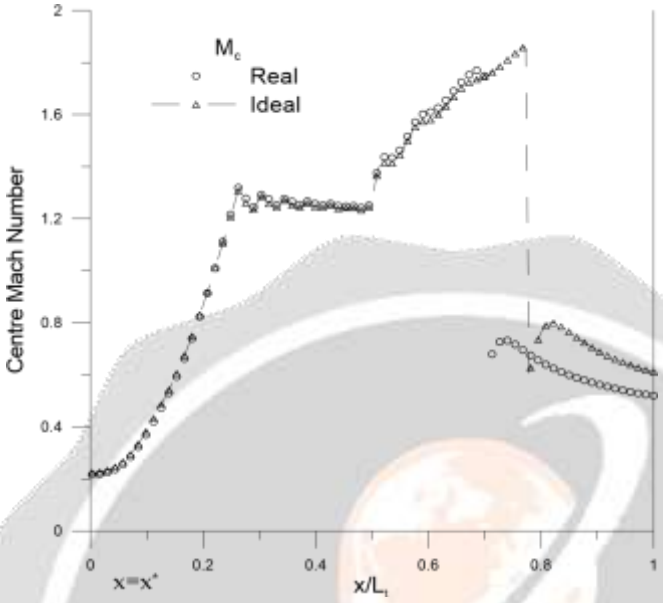

Fig. 8. To compare the performance of actual and ideal methane in an enlarged throat nozzle, we measured the centerline Mach number.

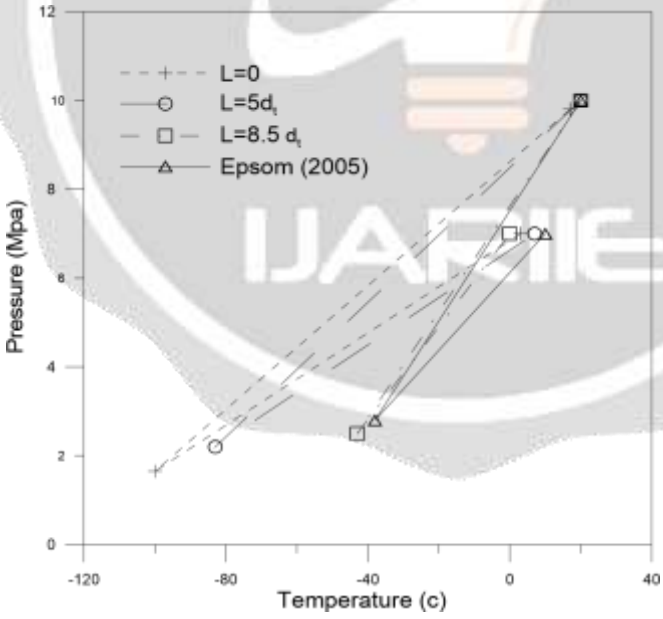

Fig. 9. Extensive throat nozzle pressure-temperature chart for actual gas (methane) simulation

To accurately anticipate the shock location, thermodynamic models and the geometry of the system play the most important roles. Since EOS accuracy is directly related to shock location and behavior, an improved EOS would be more useful.

Constant Cross Section Area Conduit Length: Twister Inc. (Epsom, 2005) employs an extended constant area throat right before the diffuser portion of the Laval nozzle to separate liquid particles from natural gas and insert instruments to regulate the shock wave position. By choosing various length-to-diameter (L/dt) ratios, we were able to investigate how long the constant cross section area conduit would need to be in order to have an impact. A pressure-temperature chart (P-T) depicts the simulation's outcomes, as seen in Figure 9. Adjusting (L/dt) would allow us to construct the same P-T graph as the Twister (Epsom, 2005) with different conduit lengths. This shows that, in addition to the nozzle output pressure, the minimum system temperature and shock position may be regulated by modifying the channel length.

Creating a mesh

It is critical to the precision and stability of the numerical calculation to have a high-quality mesh. The accuracy with which a discretization scheme may represent a grid's continuous governing equations is known as grid quality. Meshing techniques and mesh density distribution have a large impact on the ultimate accuracy and efficiency of any numerical solution. Grid generation and flow solving approaches must be properly matched to get an effective overall numerical solution. Maintaining a positive interaction between these two stages is essential. The optimization of the discretization scheme and the grid generation technique should be the obvious objective of any numerical simulation.

More precise calculations demand more CPU and memory resources to perform, even if accuracy improves with finer grids. Grid density may be increased and/or decreased depending on the changing flow field using adaptive grid refinement, one of several solutions to this problem. This allows for more efficient use of grid points, which saves time and resources. The multigrid strategy is another new strong method that takes a more complete approach to the broad issue of numerically modeling a physical phenomena by tightly connecting the grid generation and numerical solution parts of the simulation. On a coarser grid (Peyret, 1996), where computation is more cost-effective, a concept called the Multigrid method was developed to speed up the convergence of a collection of fine-grid discrete equations by calculating adjustments. The coarse-grid levels are applied iteratively to this procedure. To get to the coarsest mesh, a Multigrid cycle starts at the finest grid level and works its way up. Corrected values are progressively interpolated back to the lowest possible level and the process repeats again. Final discretization accuracy is only controlled by fine-grid discretization and coarser levels are just artifacts used to speed convergence..

If additional grid metric information is added, the accuracy of the grid might be lowered. It has been found that grid dependence investigations have revealed that the accuracy of the solution in the case of the axisymmetric nozzle flow may be improved by using smaller meshes. Our group likewise came to the same conclusion.

The simulation was run with three different numbers of mesh cells (1882, 5533, and 11 832). For each example, Table 1 indicates the number of iterations required to achieve convergence with regard to total mass error in the flow of inlet/outlet mass for each scenario. Increasing the grid size has no discernible impact on the number of iterations required to reach convergence. A coarser grid (e.g. 1882 cells) led to quicker convergence (1500 steps) than a finer grid. With each iteration, the number of iterations was increased by a factor of 2. Since the shock wave is one of the major gradient zones that demands grids to be tiny enough to minimize the flow variables from cell to cell, the uncertainty of the shock site encourages us to pick finer grids. Because it is impossible to predict where a shock will occur in advance, it is essential that a high-quality mesh be achieved across the flow domain. For this work, we used a mesh of 5533 grid cells to ensure that the flow parameters over the shock zone were uniformly distributed. In actual and ideal gas models, convergence happened after a given number of iteration steps. After 3182 iterations, the actual gas non-swirl scenario converged with a mass flow inaccuracy of roughly 4.8x10-4 percent. Remaining errors for continuity, energy, k and equations are shown in Table 2 for non-swirl real and ideal instances.

No. of Cells	**No. of Iterations**	**% errors in mass flow**
1 882	3 030	9.8×10^{-3}
5 533	3 182	4.8×10^{-4}
11 832	3 500	3.2×10^{-1}

Table 1. In simulations when there is a complete mass error in the input and output mass flow, the number of iterations necessary to reach convergence was

Case	**% Error of Inlet/Outlet Mass Balance**	**Number of Iteration Steps**	**Continuity**	**Energy**	***k***	ε
Ideal	2.0×10^{-4}	9 230	2.40×10^{-3}	1.90×10^{-3}	8.50×10^{-6}	9.60×10^{-6}
Real	4.8×10^{-4}	3 182	5.85×10^{-4}	5.58×10^{-4}	5.58×10^{-5}	6.03×10^{-5}

Table 2. Number of iterations that led to convergence with residual errors for continuity, energy, *k* and ε equations for non-swirl real and ideal cases

1.3.3 de Laval nozzles with extended U-shape throat

It is the goal of this part to come up with alternatives to the Laval nozzle arrangement outlined before in order to improve separation performance. Thus, the enlarged U-shaped part of the Laval nozzle was suggested. The three components of the nozzle are as follows:

1. The convergent subsonic segment that diverges slightly after the throat to account for the supersonic flow of the gas.

2. The centrifugal force applied to the particles is supposed to separate them into phases through a U-shaped expanded throat (gas-liquid, gas-solid, or gas-solid-liquid).

3. Cross-sectional growth necessary for pressure recovery is provided by the diverging section.

An inlet/outlet pressure ratio, a U-shaped section curvature radius, and a U-shaped section diameter ratio were all taken into account while creating this design. The centrifugal acceleration of the gas moving within the U-shaped portion was utilized as a measurement of the device's ability to produce a certain amount of phase separation, as were shock position and gas velocity inside the section.

The process fluid used in the simulations was an inviscid flow of methane. Mass, momentum, and energy conservation rules, together with a thermodynamic model adequate for predicting gas characteristics, guided the development of the governing equations.

A pilot test using compressed air as the process fluid is being developed since there are no experimental findings available for assessment reasons. Computer models will be compared to the results of the CFD simulations done under the identical circumstances.

1.3.3.1 Throat Diameter Ratio.

The flow always achieves sonic velocity near the neck, as shown in the preceding section. After the throat and before the U-shaped portion, a minor divergence is necessary to enable the flow to attain supersonic speed. If the pressure drop across the nozzle is sufficient, the Mach number at the entry to the U-shaped portion is completely dependent on the diameter ratio at this point to the throat. In order to take advantage of supersonic flow in a circular route, the diverging part of the U-shaped section is critical. Shock waves may occur in the U-shaped part despite the

fact that the nozzle's diameter remains constant throughout. This is due to the loss of energy that occurs in the U-shaped section.

This research found that the U-shaped section to throat diameter ratio of 1.2 was most successful. Thus, the diameter of the U-shaped section's constant cross-section area is 1.2 times greater than the diameter of the throat where the choke occurs. You must recognize this ratio is not the sole determining element in determining where a shock will be located. The radius of the U-shaped section's curvature and the outlet back pressure are other important considerations.

1.3.3.2 Radius of a U-shaped portion

Contrasting effects are caused by the U-shape section's curvature radius on flow. Speed and Mach number may be increased without causing a shock wave by increasing the radius of curvature, however this lowers centrifugal acceleration (Bird, 1924). Using the kinematic formula for acceleration, this can be shown rather simply:

$$a_{\text{tangential}} = \frac{V^2}{r} \qquad (4)$$

Because velocity is multiplied by two, its value outweighs the negative effect of increasing radius in this equation. Even though these supersonic separators are very tiny in size, a big radius of curvature will damage this attribute. Finally, a U-shaped section with a gradually decreasing radius profile was found to be the ideal arrangement for this project's curvature. Because of this, Figure 10 shows a curvature profile for the nozzle's U-shaped part.

The profile's radius begins at 40 units in the bottom left portion and steadily declines until it approaches 5 units at the very end (upper section).

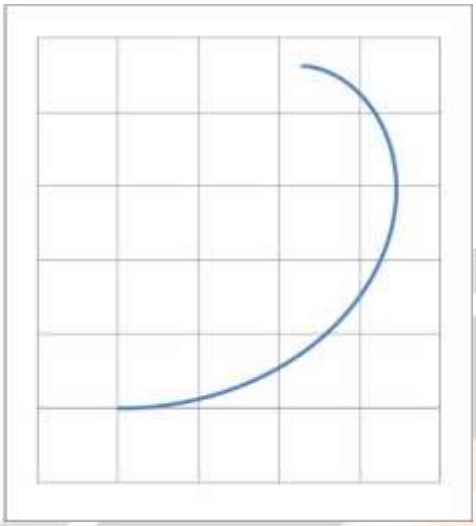

Fig. 10. The Laval nozzle's U-shaped portion has a characteristic changing curvature.

1.3.3.3 Back pressure at the outlet

The atmospheric pressure was used as the exit back pressure in this investigation. Other factors influencing the shock wave's location were intake pressure and flow rate of gas through the device, as well as the nozzle's pressure drop.

1.3.3.4 Separation of particles

The centrifugal force imposed on the flow as it travels through the U-shaped segment with high velocity causes particle separation. For example, micron size liquid droplets may be removed through a side channel that has been inserted at a suitable location in a U-shape section. Figure11 depicts the flow's experience of centrifugal acceleration along this portion. Equation is used to compute the acceleration (4). When an input pressure of 345 kPa (50 psia) was applied to the shape illustrated in Figure 12, CFD simulation results were used to construct the graph displayed in Figure 13. These particles may be seen in the graph experiencing centrifugal accelerations of up to 36,000,000 m/s2. That's around 3.7 million gallons.

1.3.3.5 The location of the shockwave

In order for these separators to function properly, the location of the shockwave is critical. According to the previous explanation, the shockwave should not occur before to or through the U-shaped part. Another consideration is how far into the diverging portion the shock occurs. To put it another way, a higher loss of pressure occurs when a shock is applied farther into this area of the device, which demands

more differential pressure driving force. The shock must occur as soon as feasible in the diverging segment.

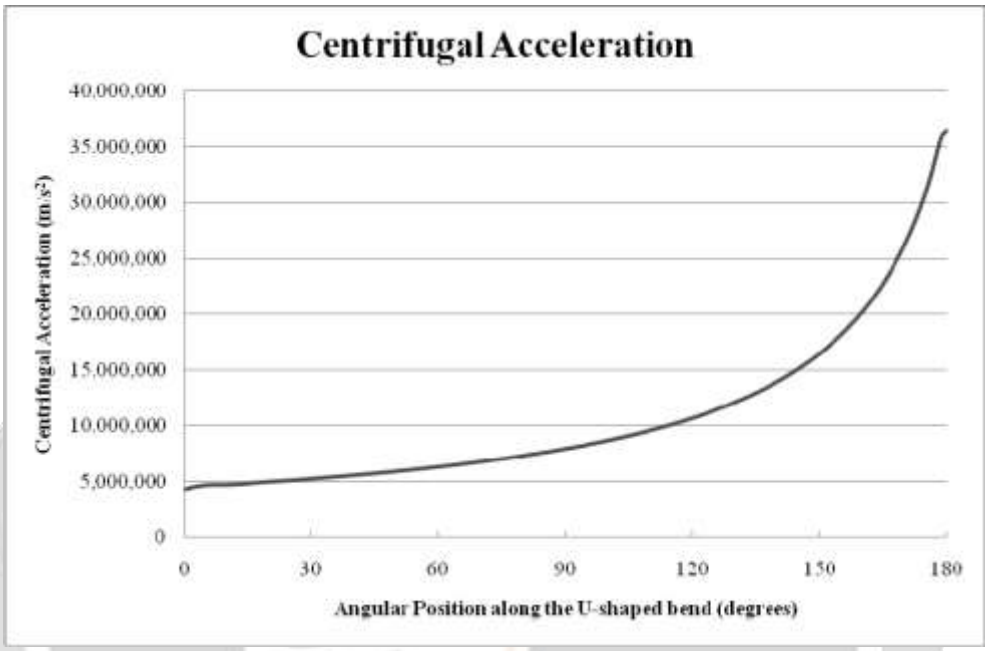

Fig. 11. Adaptation of the planned Laval nozzle's centrifugal acceleration with respect to its location along a U-shaped segment.

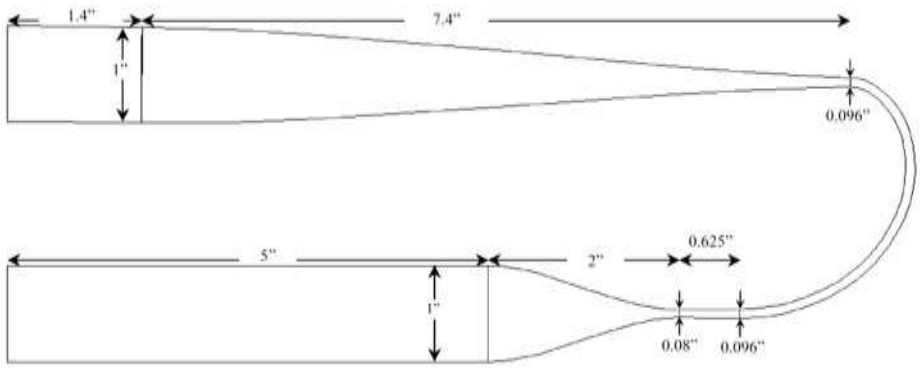

Fig. 12. A common layout for the Laval nozzle's design.

For the design and operation conditions of the separator, this quality was one of the factors that were considered. Pressure profiling and velocity profiling may be used

to determine the location of the shockwave. After using the CFD package's post-processing features, the most effective and accurate solution was Mach number contours over the device. The form and strength of the shockwave may be seen clearly in these contours (see Figure 13).

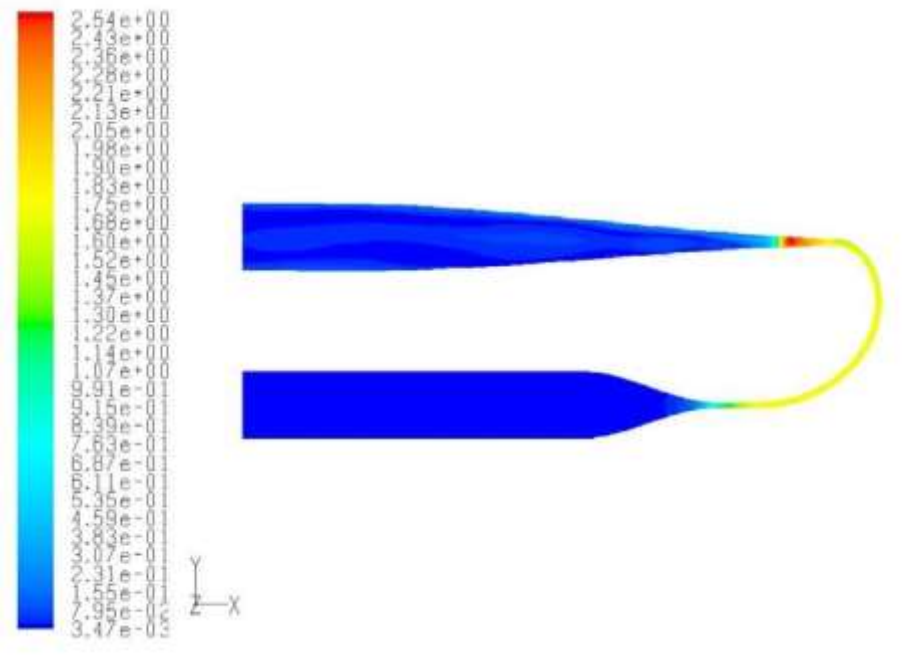

Fig. 13. Using Mach numbers, the shock wave's path may be seen.

1.3.3.6 The location of the separation channel

The location of the side channel for separating the particle flow from the main gas flow is an essential design component. The CFD package's post-processing tools make it simple to figure this out. Volume density contour in Figure 14 shows exactly where the greater density particles are concentrated in the U-shape segment.

1.3.3.7 Creation of Meshes

As previously stated, the accuracy and stability of a numerical (finite volume) analysis are directly related to the quality of the mesh. Mesh design decisions are influenced by a variety of factors such as the geometry's characteristics, the sorts of fluids involved, and the quantity of accessible memory and computing power. As seen in Figure 12, the geometry was represented by an array of wedge-shaped and tetrahedral pieces. Figure 15 shows how the geometry was broken down into six portions. Except for section 2, which had a large gradient in cross-sectional area, all

sections were meshed with wedge-shaped pieces. Stabilizing gas flow before it reaches the nozzle system is the only function of Section 1, which is a basic pipe. As a result, a fine grade mesh is not required for this section's meshing. Wedge-shaped mesh components with a length of 5.0810-3 m (0.2") are used in this part.

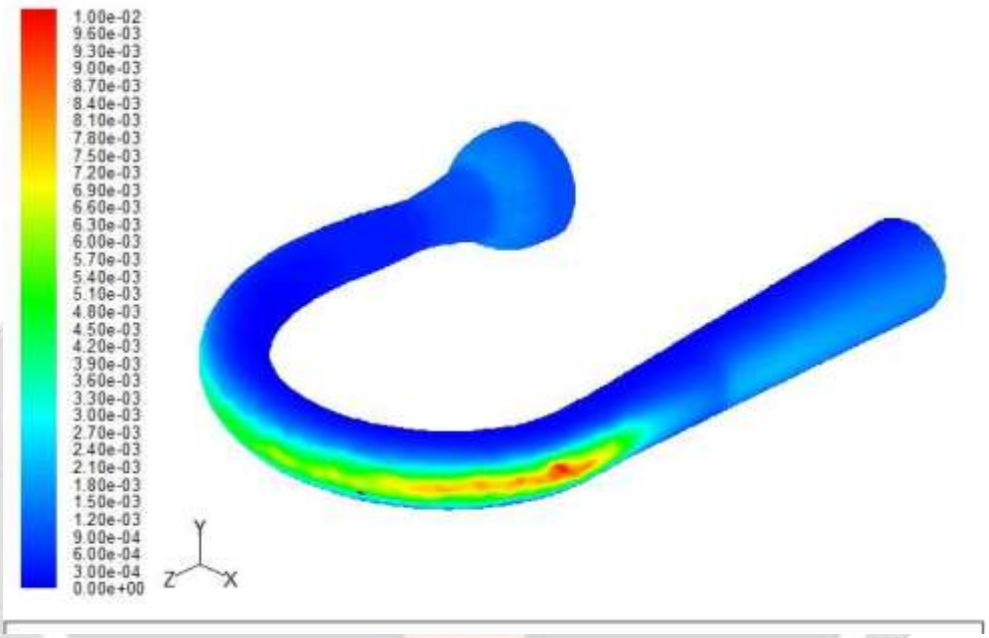

Fig. 14. Where a side channel should be placed to segregate the majority of the particles, as shown by the usual volume density contour.

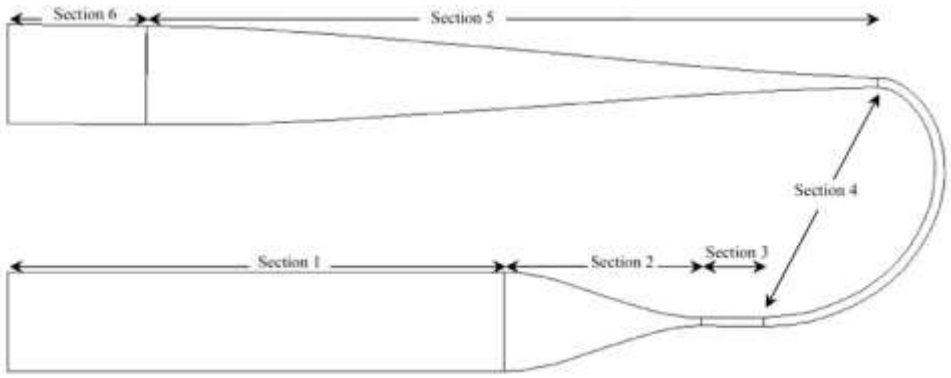

Fig. 15. Mesh-related divides in the geometry.

Triangular bases with 2.5410-3 m (0.1") long edges (see Figure 16). In the nozzle's converging portion, Section 2, the tetrahedral mesh pattern shrinks as it becomes smaller (Figures 17 and 18). The numerical analysis verifies the geometry's stability and connects the coarse mesh of part 1 to the fine mesh of section 3." A extremely tiny mesh is required in Section 3 because of the minor divergence after the throat, which allows for the gas to flow at supersonic speeds. As the cross section rises, the meshing approach uses a wedge-like member that expands laterally. There are 60 elements on the cross sectional perimeter at each point in the meshes' arrangement. To put it another way, the wedge bases start off with lateral diameters of 1.01610-4 m (0.004") and increase to 1.2710-4 m (0.005") after the throat (right before the U-shaped section). It is important to keep this portion at a consistent length of 2.5410-4 m (0.01"). A u-shaped segment may be found in Section 4. With the same base widths and lengths of 5.0810-4 m (0.02"), the wedge pieces move forward into this section. At the conclusion of this section, the wedges have grown to 2.5410-3 m (0.1") in diameter and 5.0810-3 m (0.2") in length, which is the same length as section 1. The mesh components stay the same. Although boundary layers are crucial to consider, they may be ignored since the fluids analyzed are gaseous and moving at high speeds, therefore no further attention is needed.

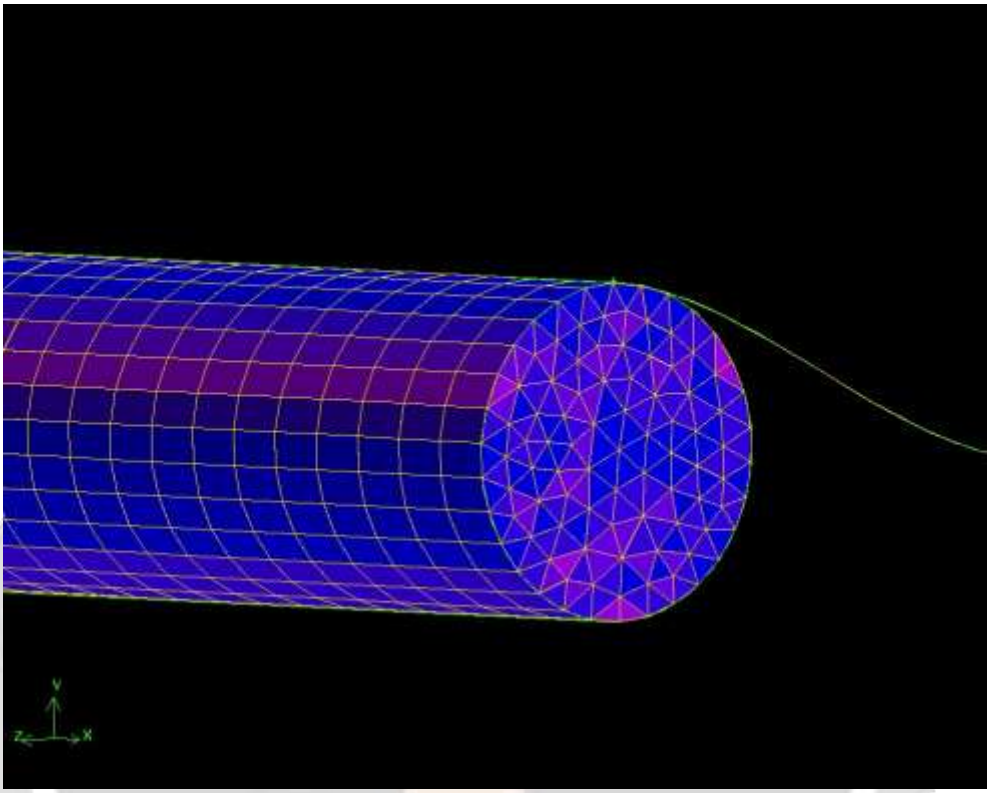

Fig. 16. The intake stabilizing part of the device is made up of wedge-shaped mesh sections (Section 1).

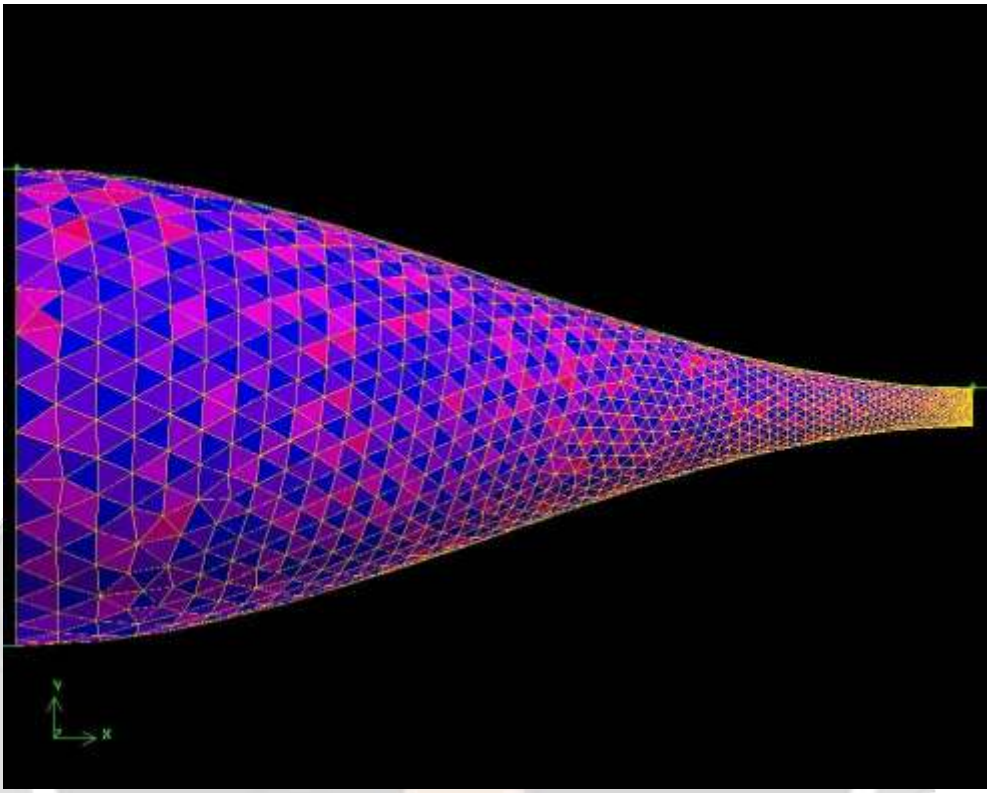

Fig. 17. The nozzle's converging portion has tetrahedral mesh components (Section 2). As they move closer to the trachea, the element volumes decrease.

1.3.3.8 Equipment for doing research

Because of the study's uniqueness and the scarcity of prior research, laboratory pilot tests were required to assess the accuracy of the CFD models. The goal was to build a nozzle system that would allow high-pressure gas to flow through it. The findings of CFD simulations of the same system would be compared to the results of pressure, temperature, and flow rate measurements taken in the real world. Figure 12 shows the geometry used in this test, and compressed air was used as the process gas. Using two aluminum blocks, two symmetrical portions of the suggested design were machined to produce the appropriate paths. If any body flaw or barrier disrupts the flow, direct pressure and temperature monitoring was out of the question. It was necessary to establish small canals at numerous spots along the journey in order to position sensors outside the fluid. 12 points of pressure and 4 points of temperature may be observed in Figure 19. The pilot test arrangement is shown schematically in Figure 20. Although the data from the measurements has yet to be examined, the early findings are in excellent accord with those from the simulations, which are still being carried out.

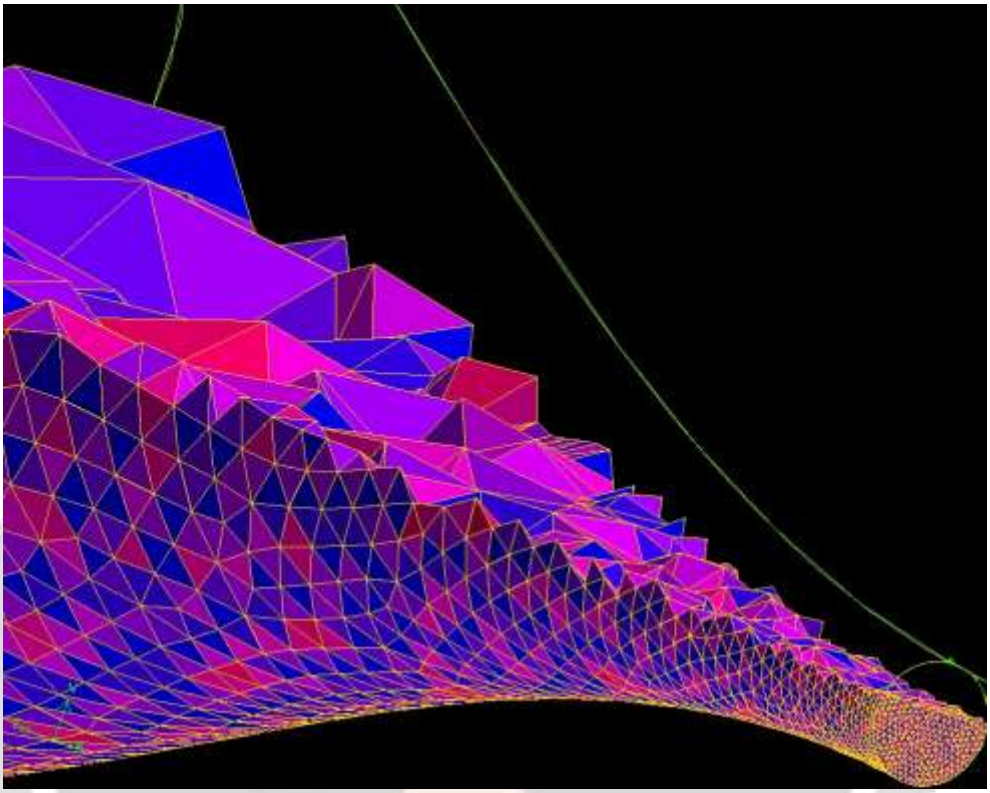

Fig. 18. View of the nozzle's converging section's mesh in planar cross-section (Section 2)

2. HIGH-PRESSURE MARINE CNG TANKS PRODUCE A COLD JET.

There might be a cold jet when a high pressure device fails and leaks through a wall fracture or the valve stem (or any other hole). CFD was utilized to examine the occurrence and its impact on the surrounding equipment.

2.1 A description of the issue

A cold jet is created when a high-pressure fluid with a low temperature is sprayed into the air via a leak or other opening at rapid speed. As a result of this phenomenon, the materials used in the high-pressure containers/vessels or pipe systems might be affected by a very low temperature. Despite the expanding need for research in this field, very few studies have been carried out to yet.

Because of the brittleness of carbon steel at such low temperatures, high-pressure tanks and pipes might fracture instantly, resulting in an explosion. The jet may also affect the strength and performance of neighboring equipment, components, and pieces.

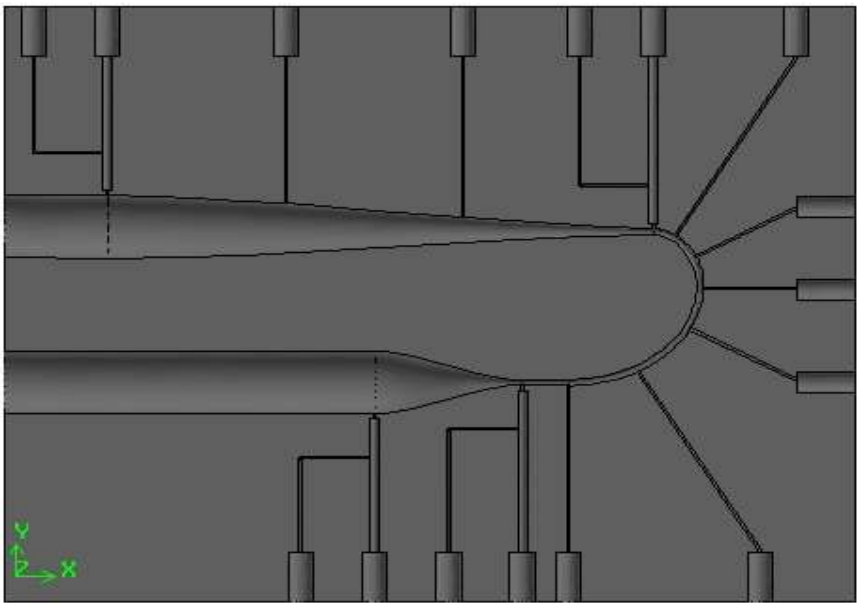

Fig. 19. The bottom of the pilot test nozzle system. Temperature sensors may be inserted into the four thicker channels. Pressure readings are made on all other channels.

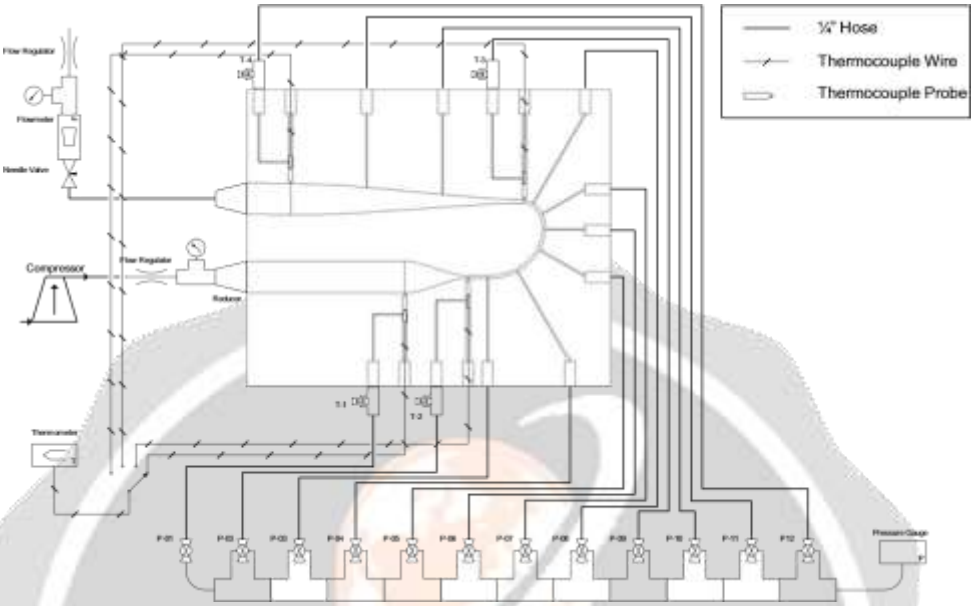

Fig. 20. Test pilot setup integrity due to temperature fluctuations is shown schematically in this process flow diagram.

The findings of this research will aid in any failure and stress analyses that may be necessary in the future.

For the purposes of this investigation, flow through the fracture, temperature distribution, and jet impact on the nearby walls were examined.

The behavior of high-pressure natural gas flowing through unintentional fissures was studied using computational fluid dynamics. It is for these reasons that we have included this area in our research:

- What happens when the crack opens?
- A crack's temperature distribution
- The impact of the jet on the walls next to the water.

2.2 Configuration and modeling of the system

Although the crack's real form may be somewhat random, we selected to use a convergent nozzle with the geometry indicated in Figure 21 for our analysis and simulations. In the high-pressure cylinders, natural gas (methane) at pressure of 122 bars and temperature of 265K was stored at 19 mm thick.

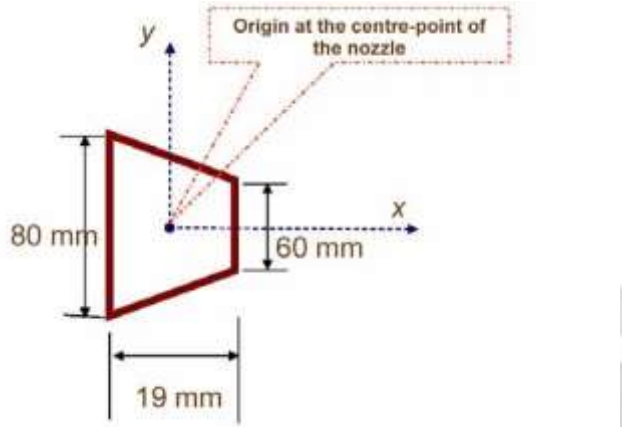

Fig. 21. Convergent Nozzle Crack Geometry Assumption

2.3 The outcomes of crack simulations

As may be seen in Figure 22, the fracture wall's Mach number varies. There are choke flow conditions near the crack outlet, which is in accordance with thermodynamics. The distance is measured from the nozzle's midpoint on the x-axis, as shown in Figure 21. The sudden reduction in pressure at the crack's exit may be explained by the gradual fall in temperature over the crack's length, which is depicted in Figure 23.

2.3.1 Crack simulation with a wall surrounding it.

By modelling the flow through the fracture in a two-dimensional environment, temperature contours may be formed around the break. Figure 24 depicts the fracture exit temperature contours on the tank's exterior wall. Because of the extreme temperature differences, the material may be put under thermal stress and eventually fail due to fatigue and failure.

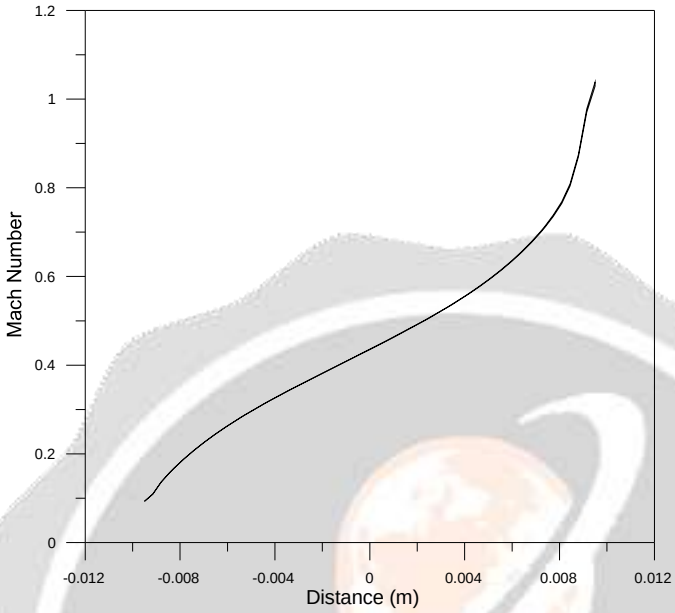

Fig. 22. Mach number at the centerline of the crack.

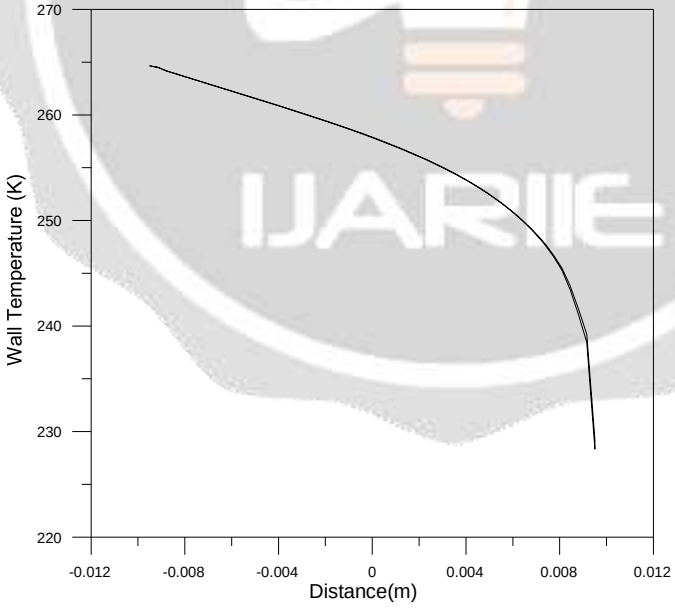

Fig. 23. Temperature variation at the inner surface of the crack

Fig. 24. The crack's temperature profile

2.4 The results of a jet simulation

Here, a natural gas jet created outside of a tank was made to strike two distant fixed walls. Figure 25 depicts the jet's velocity contours. Because of the patch of stagnation, it is possible to see where and how the flow varies. The changed stream hits the wall of the neighboring components (here another tank with the same height) and leaves a particular portion exposed to impingement under reduced strength. As a result, the temperature in this region rises.

There are three distinct temperature zones along the neighboring wall, as shown in Figures (26a and 26b):

a. The location of the encroaching point

b. The area with the greatest fluctuation

c. The area of moderate fluctuation

The jet velocity profile at the neighboring wall in Figure 25 shows that the flow gradually varies and then significantly changes its direction to become parallel to the wall as it gets closer to the adjacent wall. Consequently, stagnation or circulating flow (eddies) are in touch with the wall at a certain distance from the wall. Because of this, the temperature in this zone drops rapidly from a specific point (the stagnation spot) and then gradually rises the rest of the way down the wall.

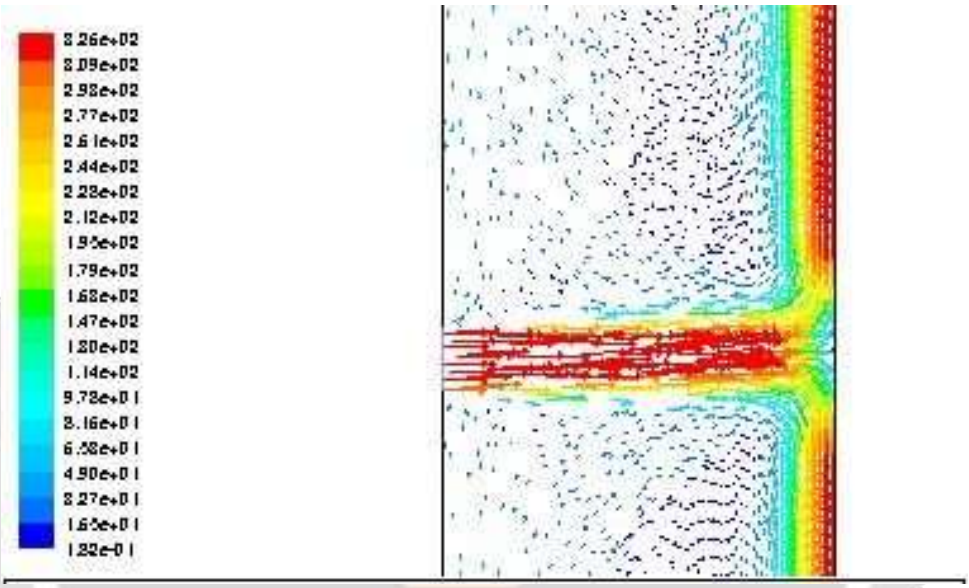

Fig. 25. Jet velocity vector caused by impinging with adjacent wall

3. CONCLUSIONS

A few key findings are as follows:

• Shockwaves have been investigated using a CFD method. Additionally, the influence of actual gas characteristics on the flow behavior were examined. When studying high-pressure natural gas flow systems, it is critical to be aware of the true gas fluid behavior. The assumption that a gas is a perfect gas may lead to serious mistakes. The comparison of ideal and actual gas models was used to show the inaccuracies associated in estimating heat, work, and other thermal processes when real attributes are disregarded. Shockwave location and design of supersonic devices might be severely harmed by the ideal gas assumption based on CFD simulations done for diverse gases.

• Geometry and vorticity were examined for their effects on vortex generation. These extended constant area areas, which link nozzle and diffuser, have been chosen because they are of relevance in separating liquid particles from each other. There was a direct correlation between changes in channel length and

changes in the shock wave location and minimum system temperature, which in turn affected droplet amount and quality if condensation occurred. When fluid enters the nozzle in a semi-tangential direction, swirls occur. Because of the high centrifugal acceleration in the nozzle throat, the centrifugal force is responsible for particle separation, and the strength and behavior of vorticity were examined. There is an acceleration of 105 or perhaps 106 times greater than this one.

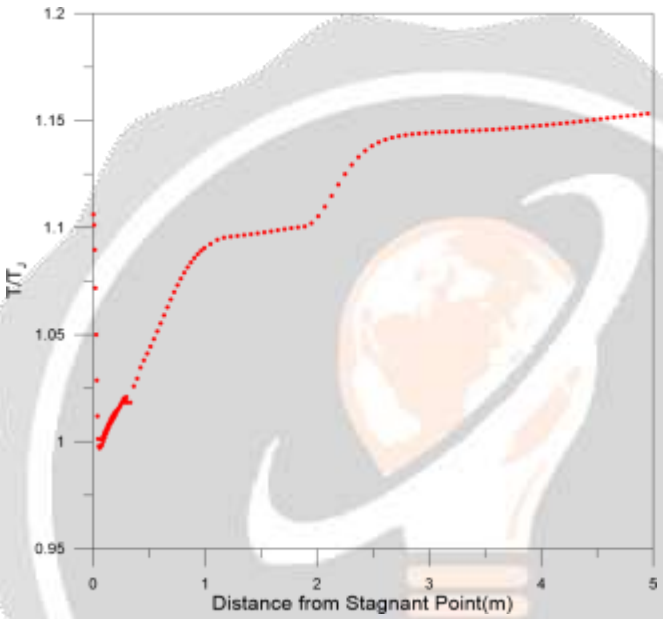

(a)

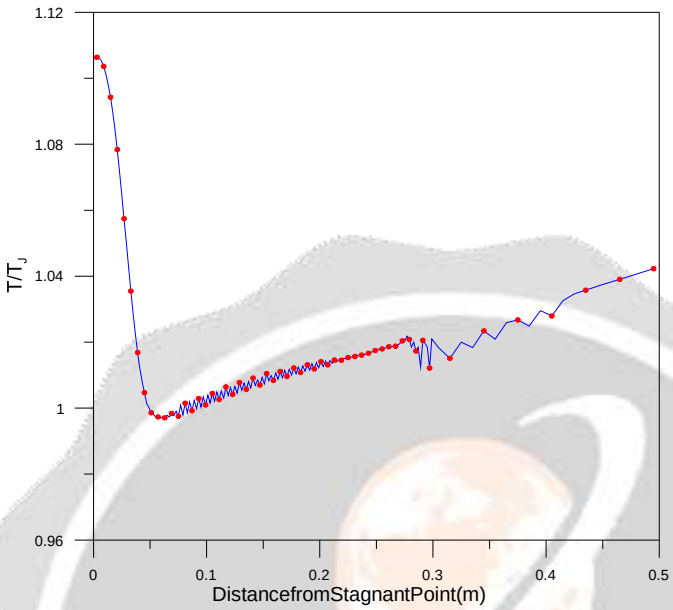

(b)

Fig. 26. is a function of distance from the stationary point: wall temperature ratio At the stagnant region, temperature profiles are shown for both the adjacent wall and the enlarged portion.

particles as tiny as a few tenths of a macron in diameter may be separated by gravity alone. It is also critical to have a firm grasp on how pressure losses throughout the system affect the economics of natural gas processing's use of supersonic nozzles. Costly compression facilities are needed to compensate for the loss of pressure. In the future, we want to integrate multiphase and multicomponent fluid systems in our research to better understand the natural gas's behavior inside the system.

• As a result, it can be said that the extended U-shaped portion of a nozzle, as opposed to a straight nozzle, may provide greater gas separation performance. A full-scale separator of this sort might theoretically reach extremely significant centrifugal forces, despite the fact that the centrifugal acceleration values measured here are greatly dependent on the geometrical size (curvature radius). Although there is no external data, CFD simulations have shown to be rather accurate. In spite of how far off in the distance it seems to be, CFD simulations have showed significant promise and promising outcomes.

Studying the flow of high-pressure gas through complicated geometries and advanced models like the impinging area is made easier by CFD simulation, which is a powerful tool. It was shown in this research that CFD can be utilized to shed

light on such occurrences, giving it a strong place among other methods. Choosing the proper thermodynamic model is critical in modeling natural gas flow under high pressure and low temperature circumstances. The results reveal that the flow shifts from subsonic to supersonic as a result of the divergent geometry of the fracture. Thus, the flow characteristics through the fracture are visibly affected by irreversibility. The cold jet's CFD modeling predicted that the jet's impact on neighboring components would be significant. Differences in temperatures between jet and adjacent wall are greater in divergent forms than convergent shapes, due to the impinging phenomenon. Furthermore, the temperature distribution is significantly altered by heat exchange caused by jet collisions with adjacent storage tanks.

ACKNOWLEDGEMENTS

The Authors are thankful to, IMO state university, Owerri Nigeria for Enabling the Research project.

REFERENCES

Alfyorov, V., Bagirov, L., Dmitriev, L., Feygin, V., Imayev S., Lacey, J. R., 2005. Supersonic Nozzle Efficiently Separates Natural Gas Components. Oil and Gas Journal.

103(20), 53-58.

Arina R., 2004. Numerical Simulation of Near-Critical Fluids. Applied Numerical Mathematics 51(4), 409-426.

Bai-Shi-I, 1961. An Introduction into Theory of Compressible Liquid Flow, Moscow: Izd. Inostrannoi Literatury, (Russ. Transl.)

Bird, R.B., 1924. Transport Phenomena. John Wiley & Sons, New York; USA.

Brouwer, J.M., Epsom, H. D., 2003. Twister Supersonic Gas Conditioning for Unmanned Platforms and Sub sea Gas Processing Source. Offshore Europe Conference - Proceedings, Aberdeen, UK, pp. 219-225.

Carvero, C., and Satta, A., 2000. A CFD Model for Real Gas Flow. ASME paper, GT-518.

Crocko, L., 1950. One-Dimensional Consideration of the Gas Dynamics of TimeIndependent Flows, in Fundamentals of Gas Dynamics, H.W. Emmons, Ed., Princeton: Princeton University Press, Princeton, USA.

Drikakis, D., Tsangaris, S., 1993. Real Gas Effect for Compressible Nozzle Flows. Journal of Fluid Engineering. 115(117), 115-120.

Ginzburg, I. P., 1939. Uch. Zap. Leningr. Gos. University, no. 42, pp. 5.

Hengwei, L., Zhonggliang, L., Yongxun, F., Keyu, G., and Tingmin,Y., 2005. Characteristic of a Supersonic Swirling Dehydration System of Natural Gas. Chinese Journal of Chemical Eng., 13(1), 9-12.

Kouremenos, D. A., 1986. Normal Shockwaves of Real Gases and the Generalized Isentropic Exponent. Forschung im Ingenieurwesen, 52(1), 23-31.

Karimi, A., and Abedinzadegan Abdi, M., 2006. Selective Removal of Water from Supercritical Natural Gas. SPE 100442, Proceedings of the SPE Gas Technology Symposium, Calgary, Alberta, Canada, 15-18.

Man, H. C., Duan, J., Yue, T. M., 1997. Design and Characteristic Analysis of Supersonic Nozzle for High Pressure Laser Cutting. Journal of Materials Processing Technology, 63(1-3), 217-222.

Molleson, G.V. and Stasenko, A. L., 2005. An Axisymmetric Flow of a Mixture of Real Gases with a Condensing Component. High Temperature, 43(3), 422-430.

Okimoto, F., Brouwer, J. M., 2002. Supersonic Gas Conditioning. World Oil, 223(8), 89-91.

Peng, D. Y., and Robinson, D. B., 1976. A New Two-Constant Equation of State. Ind. Eng. Chem. Fundam., 15, 59-64.

Pope, S. B., 2000. Turbulent Flows. Cambridge University Press. Cambridge, USA.

Redlich, O., and Kwong, J. N. S., 1949. On the Thermodynamics of Solutions. V. An Equation of State. Fugacities of Gaseous Solutions. Chem. Rev., 44, 233-244.

Saad M. A., 1993. Compressible Fluid Flow. 2nd Edition, Prentice-Hall, Inc., New Jersey, USA.

Soave, G., 1972. Equilibrium Constants from a Modified Redlich-Kwong Equation of State. Chemical Engineering Science, 27(6), 1197-1203.

Wark, K., 1995. Advanced Thermodynamics for Engineers. McGraw-Hill Series, New York, USA